

Source Coding Based Millimeter-Wave Channel Estimation with Deep Learning Based Decoding

Yahia Shabara *Student Member, IEEE*, Eylem Ekici, *Fellow, IEEE*, and C. Emre Koksal, *Senior Member, IEEE*

Abstract—The *speed* at which millimeter-Wave (mmWave) channel estimation can be carried out is critical for the adoption of mmWave technologies. This is particularly crucial because mmWave transceivers are equipped with large antenna arrays to combat severe path losses, which consequently creates large channel matrices, whose estimation may incur significant overhead. This paper focuses on the mmWave *channel estimation* problem. Our objective is to reduce the number of measurements required to reliably estimate the channel. Specifically, channel estimation is posed as a “*source compression*” problem in which measurements mimic an *encoded* (compressed) version of the channel. *Decoding* the observed measurements, a task which is traditionally computationally intensive, is performed using a *deep-learning-based* approach, facilitating a high-performance channel discovery. Our solution not only outperforms state-of-the-art compressed sensing methods, but it also determines the lower bound on the number of measurements required for reliable channel discovery.

Index Terms— Millimeter-Wave, Channel Estimation, Path Discovery, Sparse Recovery, Source Coding, Machine Learning.

I. INTRODUCTION

THE RAPID increase in mobile data traffic has motivated the exploration of mmWave spectrum bands [1]–[4]. While mmWave communication promises orders of magnitude increase in data rates, it both i) suffers from severe path losses [5] and ii) necessitates the use of power-hungry circuits to operate. To overcome these problems, large-gain, highly-directional antenna arrays are proposed as a counter measure to path losses, along with less flexible, yet energy-efficient transceivers that no longer use fully-digital beamforming. Large antenna arrays, however, create channel matrices with large dimensions, which are complex to estimate. When combined with limited transceiver capabilities, large scale channel estimation may take prohibitively long periods. Reducing the number of measurements is thus a critical step towards facilitating mmWave networks. Fortunately, this does not necessarily degrade the quality of channel estimation due to the sparse nature of mmWave channels; a feature that has been revealed by empirical measurement studies and further adopted by statistical channel models [3], [6], [7].

This work focuses on *the problem of mmWave channel estimation* with the objective of decreasing the number of required measurements. We treat this problem as that of path/beam discovery which is crucial for *initial link establishment* between a transmitter (TX) and a receiver (RX) (also known as *Initial Access*). We solve this problem using a technique inspired by *binary source coding (data compression)*. Although binary codes are natively designed to compress binary data, we provide a foundation for the same codes to

be used for compressing complex-valued data, as well. We devise a method to obtain channel measurements such that they resemble a compressed version of the channel matrix. To estimate the channel from the acquired measurements, we train a Deep Neural Network (DNN) that enables very high speed processing. This method is also unique in the sense that it reduces the problem of estimating the *channel matrix* as a whole into several smaller sub-problems of estimating the individual rows and columns of that matrix. The key contributions of this work are as follows:

- We show that lossless, fixed-rate, linear source codes can be used to design efficient channel measurements that can be *uniquely* mapped to the underlying channels.
- We accurately evaluate the number of measurements needed for reliable channel discovery (as opposed to a mere scaling law). This number is dependent on the compression ratio of the chosen code.
- We present a tight lower bound on the number of measurements needed to reliably discover the channel and provide a solution that achieves this bound.
- We propose a high-performance DNN based measurement-to-channel mapping.
- We show that our solution outperforms the state-of-the-art compressed sensing based solutions and the IEEE 802.11ad beam alignment method.

The mmWave channel estimation problem can generally be divided into two intertwined parts. The first is: *how to obtain “good” measurements that can be used to reliably discover the channel?* and the second is: *how to map these measurements to corresponding channel estimates?* Motivated by our proposed solution, we name these two parts “*Channel Encoding*” and “*Measurement Decoding*”, respectively. Encoding and decoding are intertwined because a selection of a specific decoding method often dictates (i) how the measurements are obtained, and (ii) the number of measurements for which this specific decoding method would yield “good” performance. The dissociation of encoding and decoding as two sub-problems can be seen across almost all mmWave channel estimation research, albeit not always explicitly mentioned. This distinction, however, facilitates the identification of key aspects upon which we could improve the quality of channel estimation.

A well-known classification of encoding paradigms is encoding *with* vs. *without* feedback. Non-feedback encoding is better suited for simultaneous multi-user channel estimation, hence is scalable, while feedback-based encoding operates better at low SNR [8]. Different decoding algorithms are also

needed for these two types. This paper focuses on encoding without feedback.

The state-of-the-art mmWave channel estimation algorithms rely on compressed Sensing (CS) to reduce the number of channel measurements [9]–[12]. Other approaches include: i) measurements with hierarchical beam patterns that sequentially narrow down the angular direction(s) which contain strong propagation paths, ii) measurements with overlapped beam patterns where each measurement combines signals received from a randomly selected set of angular directions [13], and iii) machine learning based algorithms for sparse recovery of mmWave channels [14]–[17]. Further, in [18] we first introduced the idea of exploiting *binary codes* for tackling mmWave channel estimation. In particular, we exploit the capability of error discovery of channel codes and construct an analogy to path discovery in mmWave channels.

Notations: x is a scalar quantity, while \mathbf{x} is a vector and \mathbf{X} is a matrix. The transpose of a matrix is denoted by \mathbf{X}^T , while \mathbf{X}^* denotes its conjugate and \mathbf{X}^H denotes the conjugate transpose.

II. RELATED WORK

Initial Access: The “Initial Access” problem is concerned with finding the angular bearings of one or more propagation paths between a pair of TX and RX nodes, without prior knowledge about previous channel values. In mobile environments, these angular directions are expected to change after Initial Access. “Beam Tracking” methods are commonly used to correct for smaller angular changes and maintain the viability of active link(s) [19], [20]. Nonetheless, due to the narrow beams at both TX and RX, established communication links are prone to blockage (by objects in the communication environment, and even the users themselves). Hence, the initial link establishment stage might need to be repeated multiple times during every communication session. This results in high overhead to establish coherent beams during the course of the session, if the initial access process is inefficient. This paper focuses on the Initial Access problem.

Compressed Sensing (CS): CS has been a dominant approach for tackling mmWave channel estimation problems. CS strives to recover an unknown *sparse vector* \mathbf{q}^a using a small number of measurements (compared to the sparse vector dimensions). Measurements in CS, denoted by \mathbf{y} , are modeled as $\mathbf{y} = \mathbf{B}\mathbf{q}^a$, where \mathbf{B} is the sensing matrix. The *sensing matrix* is what determines the relationship between \mathbf{q}^a and \mathbf{y} . Hence, \mathbf{B} is a linear transformation that amounts to encoding \mathbf{q}^a . Sparse recovery algorithms, on the other hand, amount to decoding \mathbf{y} .

To obtain “good” measurements (which best preserve the information contained in the channel matrix), the sensing matrix need to be stochastically optimized based on criteria like the spark(\mathbf{B}) (i.e., minimum number of linearly dependent columns), the mutual coherence and the Restricted Isometric Property. Unlike standard CS problems, however, the mmWave sensing matrix is a function of the transmit precoding and receive combining vectors. Hence, the sensing matrix elements cannot be independently chosen. It is not immediately clear how a specific choice of precoders and combiners would affect

the structure of \mathbf{B} , and therefore, the performance of sparse recovery. Extending the design principles of sensing matrices from core CS theory to mmWave channel estimation is thus not straightforward and remains an open area of research.

Existing research on CS-based estimation relies on arbitrary choices of precoding and combining vectors. Specifically, uniformly distributed phase shifts are used in [21], [22]. When this solution is incorporated in mmWave channel estimation, it translates into designing antenna beam patterns of highly irregular shapes (see Fig. 9). Such beam patterns are sensitive to variations of received signal power, thermal noise and resolution of ADCs and phase-shifters. Our proposed source-coding-based solution overcomes these limitations by imposing better antenna patterns.

Developing efficient sparse recovery algorithms for CS-based mmWave channel estimation is a rich area of research. Various algorithms have different computational complexities, recovery performance, favorable range of signal to noise ratio (SNR), etc. A comparison between several classes of sparse recovery algorithms is provided in [22]. These include convex relaxation (e.g. l_1 norm minimization), greedy iteration (e.g. Orthogonal Matching Pursuit (OMP)) and Bayesian Inference. Other algorithms also include Approximate Message Passing (AMP) [23] and its variants [24], as well as machine learning based sparse recovery [25].

The number of required measurements is commonly characterized as an order of magnitude. For instance, several state-of-the-art sparse recovery algorithms require $O(L \log(\frac{n}{L}))$ measurements, where n is the number of dimensions of the sparse vector and $L \ll n$ is its sparsity level [9], [11]. This, however, is just a scaling law, which by definition, works in the asymptotic regime and is missing the constant scaling coefficient. Our proposed solution, however, accurately specifies the required number of measurements (based on n and L).

Machine Learning: Deep learning is very powerful in extracting patterns from large amounts of data. It has been widely used in problems of computer vision, speech recognition and natural language processing. Recently, it has also been applied to problems in communications [26], including, but not limited to channel estimation [15]–[17]. For instance, in [17] the beamforming vectors at the TX and RX are “learned” based on uplink pilot signals simultaneously received at multiple base stations. The base stations share their received information on a cloud, on which data processing is performed. This idea, however, is critically dependent on a dense deployment of base stations. In [15], [16], deep learning is leveraged to ease the burden of heavy computations that would otherwise be required for measurement processing.

Coding: Exploiting source codes for mmWave channel estimation has not been studied before. Our earlier work in [18] drew an analogy between *path discovery* in mmWave channels and *error discovery* in *Linear Block Channel Codes* (LBC). There exists a *duality* between the error discovery problem of channel codes and linear source compression. That is, we can use LBCs as *linear* source compression codes, as well. Nonetheless, the channel coding analogy did not naturally lend itself to characterizing the lower bound on the required number of measurements. This paper differs from

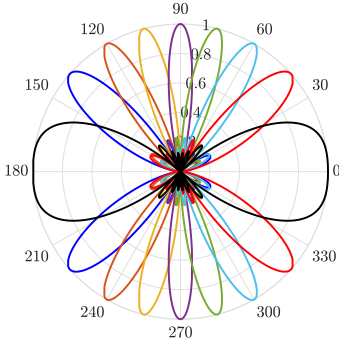


Fig. 1: Antenna sectors corresponding to angular directions $\{d_i\}_{i=1}^8$.

[18] in the following:

- Channel measurements are envisaged as compressed versions of the channel, which are obtained based on lossless, fixed-rate, linear source codes.
- The lower bound on the achievable number of measurements is accurately characterized using the entropy of the direction of the strong reflectors (in a stochastic spatial model). This not only provides a precise metric to quantify the efficiency of a used code, but it also provides a benchmark for evaluating other measurement schemes.
- A DNN-based measurement decoding is proposed and evaluated against the more computationally complex “search” method of [18].
- A comparison to compressed sensing based mmWave channel estimation is provided, demonstrating the superiority of our proposed approach.

Hashed Beams: An idea of direction inclusion/exclusion used to generate antenna patterns was adopted in [13]. Specifically, every measurement combines signals coming from a *randomly* chosen set of angular directions. This describes the encoding part and it resembles a *random* binary code. For decoding, a threshold-based decision determines whether a strong propagation path exists (i.e., it exists in one of the directions of the corresponding chosen set for this measurement). The direction which was most frequently included in the measurements that revealed a strong path is declared as the angular direction of the strongest channel path. This method discovers one path, and requires $O(L \log(n))$ measurements.

In our proposed approach, however, the angular directions whose respective beams are overlapped are *precisely determined* using a carefully chosen code. We also use a more sophisticated decoding method which makes our solution capable of discovering multiple channel paths. It also guarantees a lower number of measurements since a randomly chosen code is not expected to outperform a carefully designed one.

III. MOTIVATING EXAMPLE

Consider an RX equipped with an antenna array which can form 8 distinct beams. These 8 beams divide the angular space into resolvable directions, i.e., d_1, d_2, \dots, d_8 , as shown in Fig. 1. The RX needs to establish a Line of Sight (LoS) communication link with TX. This requires some sort of “searching” over the angular space at both TX and RX. For ease of illustration, let us reduce the link establishment

TABLE I: Channel measurements \mathbf{y}^s corresponding to all $\mathbf{q}^a \in \mathcal{Q}^a$

Angular Channel \mathbf{q}^{aT}	Channel measurement \mathbf{y}^{sT}
d_0	[0 0 0 0 0 0 0 0]
d_1	[1 0 0 0 0 0 0 0]
d_2	[0 1 0 0 0 0 0 0]
d_3	[0 0 1 0 0 0 0 0]
d_4	[0 0 0 1 0 0 0 0]
d_5	[0 0 0 0 1 0 0 0]
d_6	[0 0 0 0 0 1 0 0]
d_7	[0 0 0 0 0 0 1 0]
d_8	[0 0 0 0 0 0 0 1]

problem to that of “Angle of Arrival (AoA) discovery” at RX by assuming that TX transmits its signals omnidirectionally. Let the path gain of LoS be denoted by α , which can take arbitrary values. For simplicity of notation, let us assume $\alpha = 1$.

Our *objective* is: Find the specific direction d_{i^*} which contains the LoS path to TX using the *least possible number of measurements*. To do so, we envisage the measurement process as *lossless, fixed-rate channel compression*. This enables *harnessing the power of source compression codes to minimize the number of measurements*. It also enables deriving lower bounds on the number of measurements, using which we can accurately find the LoS (or conclude it is blocked). We propose a measurement approach which has a *predetermined* measurement sequence that (1) does not require feedback and (2) is capable of finding the LoS path, no matter in which d_i it exists. Therefore, a constant number of measurements, denoted by m , is needed for all d_i .

The key idea of LoS discovery using non-feedback linear source coding is to: 1) Construct a *binary* codebook that represents the angular channel, 2) Find a proper fixed-rate linear source code that can losslessly compress all codewords in that codebook, and 3) Use this code to design the measurements. These steps can be described as follows: **i)** Constructing the codebook is as easy as finding all possible *binary* vectors that represent the LoS position. Since $\alpha = 1$, this codebook is exactly the set of all possible channel vectors. Let the channel between TX and RX be denoted by \mathbf{q}^a , and let \mathcal{Q}^a be the set of all possible channels. The channel $\mathbf{q}^a \in \mathcal{Q}^a$ has 8 components; each one represents the path gain corresponding to a unique angular sector as shown in Fig. 1. Table I shows each possible \mathbf{q}^a in our setup (for arbitrary gain values, simply replace any ‘1’ in Table I with α). **ii)** Choose the linear source code, denoted by its generator matrix \mathbf{G} as follows

$$\mathbf{G} = \begin{pmatrix} 1 & 0 & 0 & 0 & 1 & 0 & 0 & 1 \\ 0 & 1 & 0 & 0 & 1 & 1 & 0 & 1 \\ 0 & 0 & 1 & 0 & 0 & 1 & 1 & 0 \\ 0 & 0 & 0 & 1 & 0 & 0 & 1 & 1 \end{pmatrix} \quad (1)$$

To compress \mathbf{q}^a , we simply need to find the matrix multiplication $\mathbf{y}^s = \mathbf{G}\mathbf{q}^a$ (see Table I). **iii)** Design the measurements such that \mathbf{y}^s is imitated by the measurement results. **This is done by beamforming at RX.** Notice that the i^{th} measurement, i.e., y_i^s (the i^{th} component of \mathbf{y}^s) is the multiplication of the i^{th} row of \mathbf{G} by \mathbf{q}^a . Mathematically, this is just adding all elements q_j^a of \mathbf{q}^a which corresponds to $g_{i,j}=1$, ($g_{i,j}$ is the

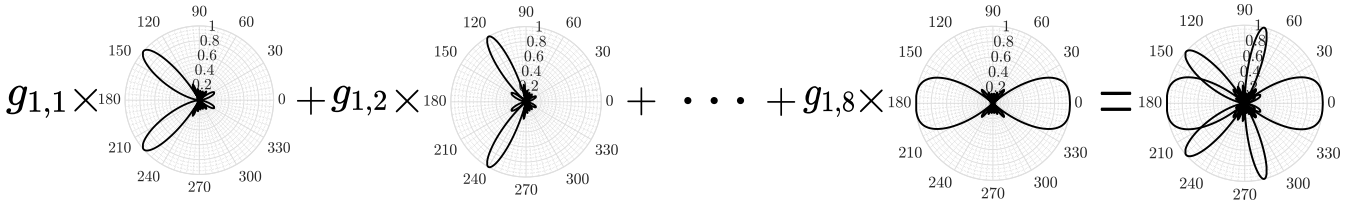


Fig. 2: Generating the beam pattern required for the 1st measurement (y_1^s)

element at row i , and column j in \mathbf{G}). That is

$$y_i^s = \sum_{j=1}^8 q_j^a \times g_{i,j} = \sum_{j: g_{i,j}=1} q_j^a. \quad (2)$$

Hence, measurement i should only contain the directions d_j whose corresponding $g_{i,j}$ equals 1, and exclude the rest (Notice that we can map the i^{th} row of \mathbf{G} to the i^{th} measurement and the j^{th} column to the j^{th} sector (direction d_j)). Essentially, this means that in each of the measurements y_i^s , we combine the signals received at a specific set of AoA directions. This can be realized by carefully shaping the antenna pattern using beamforming. Fig. 2 highlights this process for the 1st measurement in which only the direction d_1, d_5 and d_8 are included. The measurement results $\forall d_i$ are shown in Table I. Note that the number of required measurements is 4 for all d_i .

Lower Bound: A fundamental question that arises here is: *Can we find a better fixed-rate, lossless source code (other than the one given in Eq. (1)) that would produce fewer measurements, and hence increase the efficiency of the measurement process?* To answer this question, we need to find **the minimum expected number of measurements** required to discover the channel using our proposed source coding solution. This number is identical to the minimum average code length (over all fixed-rate, lossless codes). The minimum average code length is well-known to be lower bounded by the **Shannon Entropy**; denoted by H_2 and defined as

$$H_2(\mathbf{q}^a) = \sum_{\mathbf{q}^a \in \mathcal{Q}^a} \mathbb{P}(\mathbf{q}^a) \log_2 \left(\frac{1}{\mathbb{P}(\mathbf{q}^a)} \right) \quad (3)$$

Calculating $H_2(\mathbf{q}^a)$ requires knowledge of the probability distribution $\mathbb{P}(\mathbf{q}^a)$. Fixed-rate codes, however, do not account for the frequency of \mathbf{q}^a (hence, the mapping to equal-length codes). By limiting the space of codes to be over fixed-rate codes, we can improve the bound to be

$$\lceil \log_2(|\mathcal{Q}^a|) \rceil \geq H_2(\mathbf{q}^a) \quad (4)$$

where $|\mathcal{Q}^a| = 9$ (recall that there exists 9 possible scenarios for \mathbf{q}^a as shown in Table I). This tighter bound is obtained by assuming a *Uniform* distribution, which is the entropy maximizing distribution, over the channel space \mathcal{Q}^a . Eq. (4) reveals that our chosen code achieves the lower bound of 4 measurements. We provide a formal discussion on the lower bound in Section V-C.

IV. SYSTEM MODEL

We consider point-to-point mmWave channels with n_t and n_r antennas at TX and RX, respectively. Antennas at TX and RX form Uniform Linear Arrays (ULA). Generalization to

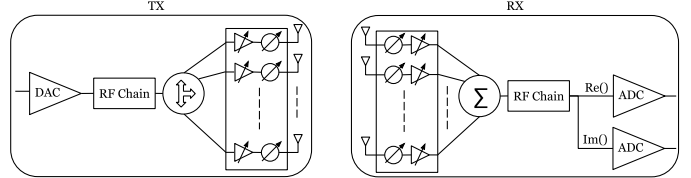


Fig. 3: Transceiver architecture: At TX, an n_t -way power splitter divides the transmit signal which is then passed through variable-gain amplifiers and phase-shifters. A single DAC is required since TX sends real valued signals. At RX, the acquired signal is passed through a similar network of power amplifiers and phase-shifters before being combined and fed to a single RF chain. Two ADCs are required to obtain I/Q components of received signals.

Uniform Planar Arrays is straightforward but not considered in this paper for simplicity. Every antenna element is connected to a phase-shifter and a low-power variable-gain amplifier. On the TX side, a single RF chain feeds its ULA through an n_t -way power splitter, while on the RX side, the outputs of the ULA, after being processed by amplifiers and phase-shifters, are then linearly combined using an adder and fed through to a single RF chain with in-phase (I) and quadrature (Q) channels. Two mid-tread ADCs with 2^b+1 levels are used to quantize the I and Q components of the received signal. The term b loosely denotes the number of bits that describe the ADC resolution. Fig. 3 depicts the transceiver architecture.

We assume single-tap channels where all channel paths have just one significant tap. We also adopt a channel clustering model where paths between TX and RX form clusters in the angular domain [1], [6]. Let L denote the number of available channel clusters. Due to the sparse nature of mmWave channels, only a limited number of clusters exist¹, where $L \ll n_r, n_t$. Since distinct paths within each cluster cannot typically be resolved, we assume that each cluster contains only one path. Each channel path (e.g., l^{th} path) is attributed with an AoD θ_l , an AoA ϕ_l and a path gain α_l . Let $\alpha_l^b \in \mathbb{C}$ denote the baseband path gain such that

$$\alpha_l^b = \alpha_l \sqrt{n_r n_t} e^{-j \frac{2\pi \rho_l}{\lambda_c}}, \quad (5)$$

where ρ_l is the path length and λ_c is the carrier wavelength. We define the *directional cosines* of the AoD and AoA of the l^{th} path as $\Omega_{tl} \triangleq \cos(\theta_l)$ and $\Omega_{rl} \triangleq \cos(\phi_l)$, respectively. The transmit and receive spatial signatures at an arbitrary directional cosine Ω is denoted by $e_t(\Omega)$ and $e_r(\Omega)$, respectively.

¹Prior knowledge about the number of clusters can be obtained from statistical channel information, which in turn are obtained from channel measurement campaigns. For instance, measurements carried out in New York City revealed that an average number of 2 or 3 clusters exists in mmWave channels at 28 and 73 GHz [3].

We define $\mathbf{e}_t(\Omega)$ (and similarly $\mathbf{e}_r(\Omega)$) as:

$$\mathbf{e}_t(\Omega) = \frac{1}{\sqrt{n_t}} \left(1, e^{-j2\pi\Delta_t\Omega}, e^{-j2\pi2\Delta_t\Omega}, \dots, e^{-j2\pi(n_t-1)\Delta_t\Omega} \right)^T \quad (6)$$

where Δ_t and Δ_r are the antenna separations at TX and RX ULAs, normalized by λ_c .

Let $\mathbf{Q} \in \mathbb{C}^{n_r \times n_t}$ denote the channel matrix such that

$$\mathbf{Q} = \sum_{l=1}^L \alpha_l^b \mathbf{e}_r(\Omega_{rl}) \mathbf{e}_t^H(\Omega_{tl}). \quad (7)$$

The corresponding angular channel of \mathbf{Q} , whose rows and columns divide the channel into resolvable RX and TX angular bins, respectively, is denoted by \mathbf{Q}^a and can be obtained as:

$$\mathbf{Q}^a = \mathbf{U}_r^H \mathbf{Q} \mathbf{U}_t. \quad (8)$$

If n_t or n_r equals 1, \mathbf{Q} and \mathbf{Q}^a are reduced to vectors which we denote by \mathbf{q} and \mathbf{q}^a , respectively. The matrices \mathbf{U}_t and \mathbf{U}_r are the transmit and receive *unitary Discrete Fourier Transform (DFT)* matrices whose columns form an orthonormal basis for the transmit and receive signal spaces \mathbb{C}^{n_t} and \mathbb{C}^{n_r} , respectively. The definition of \mathbf{U}_t (likewise for \mathbf{U}_r) is given as [27, Chapter 7.3.4]

$$\mathbf{U}_t \triangleq \left(\mathbf{e}_t(0) \quad \mathbf{e}_t\left(\frac{1}{L_t}\right) \quad \dots \quad \mathbf{e}_t\left(\frac{n_t-1}{L_t}\right) \right), \quad (9)$$

where $L_t = n_t \Delta_t$ ($L_r = n_r \Delta_r$) denote the length of the TX (RX) antenna array, normalized by λ_c .

Similar to [11], [28], [29], we assume perfect sparsity where channel paths lie along AoD and AoA directions defined in \mathbf{U}_t and \mathbf{U}_r . Hence, each path only contributes to a single component of \mathbf{Q}^a . Thus, only L (possibly less) non-zero components in \mathbf{Q}^a exists. The baseband model is

$$\mathbf{u}_b = \mathbf{Q} \mathbf{x} + \mathbf{n} \quad (10)$$

where \mathbf{u}_b is the received vector at RX front-end while $\mathbf{n} \sim \mathcal{CN}(\mathbf{0}, N_0 \mathbf{I}_{n_r})$ is an i.i.d. complex Gaussian noise vector. TX sends pilot symbols s , with power P , which are processed using precoders $\mathbf{f}_j \in \mathbb{C}^{n_t}$ to obtain the transmit vectors $\mathbf{x} = \mathbf{f}_j s$. Hence, the transmit SNR is

$$\text{SNR} \triangleq \frac{P}{N_0} \times \mu, \quad (11)$$

where μ is the path loss. The rx-combining vectors $\mathbf{w}_i \in \mathbb{C}^{n_r}$ are used to obtain the received symbols $u_{i,j}$ such that

$$u_{i,j} = \mathbf{w}_i^H \mathbf{Q} \mathbf{f}_j s + \mathbf{w}_i^H \mathbf{n}, \quad \text{where } i \in \{1, \dots, m_r\}, j \in \{1, \dots, m_t\} \quad (12)$$

Finally, a quantized version $u_{i,j}^s$ of $u_{i,j}$ is obtained such that

$$u_{i,j}^s = [\mathbf{w}_i^H \mathbf{Q} \mathbf{f}_j s + \mathbf{w}_i^H \mathbf{n}]_+ \quad (13)$$

where $[\cdot]_+$ represents the quantization function. The noise component, normalized by $\|\mathbf{w}_i\|$ has a complex Gaussian distribution, i.e., $\frac{\mathbf{w}_i^H \mathbf{n}}{\|\mathbf{w}_i\|} \sim \mathcal{CN}(0, N_0)$.

Let $y_{i,j}^s = \mathbf{w}_i^H \mathbf{Q} \mathbf{f}_j s$ denote the error-free measured symbols and let $z_{i,j} = u_{i,j}^s - y_{i,j}^s$ denote the *measurement error* which includes both **channel noise** and **quantization error**.

A. Problem Formulation

The problem we need to solve is to minimize the number of measurements $m = m_t \times m_r$ such that \mathbf{Q} can be reliably reconstructed. This problem can be mathematically stated as:

$$P1: \underset{\mathbf{w}_i, \mathbf{f}_j, \mathcal{D}}{\text{minimize}} \quad m_t \times m_r \quad (14a)$$

$$\text{subject to} \quad y_{i,j}^s = \mathbf{w}_i^H \mathbf{Q} \mathbf{f}_j, \quad (14b)$$

$$\mathcal{D}(\{y_{i,j}^s\}) = \mathbf{Q}^a \quad (14c)$$

Note that $y_{i,j}^s$ exists $\forall i, j \in \{1, \dots, m_r\} \times \{1, \dots, m_t\}$. That is, measurements are taken using all combinations of \mathbf{f}_j and \mathbf{w}_i . We also use $s = 1$. The design variables are the tx-precoders \mathbf{f}_j , the rx-combiners \mathbf{w}_i and the decoding function \mathcal{D} . We do not explicitly consider the impact of errors in this formulation but its effect will be studied in Section V-D.

V. SOURCE-CODING-BASED MEASUREMENTS

In this section, we formally introduce *mm-wave beam discovery* as a source coding problem. We initially focus on channels with single-transmit, multiple-receive antennas. Specifically, we provide the conditions under which a chosen fixed-rate source code can be used to uniquely “*encode*” channel vectors in \mathbb{C}^{n_r} into measurement vectors of fewer components. This setting is **identical to that of multiple-transmit, single-receive antennas**. In Section VI, we show how to use DNNs to “*decode*” the measurements and obtain an estimate for the observed channel. Then, in Section VII, we consider general channels with multiple TX and RX antennas. Now, let us start with the following discussion on source codes.

A. Source Codes

Let C be a binary *linear* source code with encoding and decoding functions denoted by $\mathcal{E}_{\mathbb{F}_2}$ and $\mathcal{D}_{\mathbb{F}_2}$, respectively. We refer to C as the encoding-decoding function pair $(\mathcal{E}_{\mathbb{F}_2}, \mathcal{D}_{\mathbb{F}_2})$. The subscript \mathbb{F}_2 denotes the finite field of two elements $0_{\mathbb{F}_2}$ and $1_{\mathbb{F}_2}$ (also referred to as *GF(2)*) over which the code C is defined. Later on, we will drop the subscripts to simplify notation as long as they can be inferred from the context.

Definition V.1 (Linear Source Code). A source code C whose encoding function $\mathcal{E}_{\mathbb{F}_2}$ is a linear function of the source sequences is called a **linear source code**.

Let \mathbf{s} be a source sequence of length n where $\mathbf{s} \in \mathcal{S} \subseteq \{0_{\mathbb{F}_2}, 1_{\mathbb{F}_2}\}^n$, and let $\mathbf{c}_s \in \mathcal{I}_S \subseteq \{0_{\mathbb{F}_2}, 1_{\mathbb{F}_2}\}^m$ be its associated binary representation under C where \mathcal{I}_S is the image of \mathcal{S} under $\mathcal{E}_{\mathbb{F}_2}$. Thus, using a linear source code C , we can find the representation of \mathbf{s} under C using

$$\mathbf{c}_s = \mathbf{G} \mathbf{s}, \quad (15)$$

where $\mathbf{G} \in \{0_{\mathbb{F}_2}, 1_{\mathbb{F}_2}\}^{m \times n}$ is called the **generator matrix**. Note that linearity guarantees fixed-rate since the code length is a constant value.

The decoding function $\mathcal{D}_{\mathbb{F}_2}$, maps sequences \mathbf{c}_s to a corresponding source sequence $\hat{\mathbf{s}} \in \hat{\mathcal{S}} \subseteq \{0_{\mathbb{F}_2}, 1_{\mathbb{F}_2}\}^n$. Suppose that \mathcal{S} is the set of all sequences such that if $\mathbf{s}_1, \mathbf{s}_2 \in \mathcal{S}$, we have that $\mathbf{s}_1 \neq \mathbf{s}_2 \iff \mathbf{c}_{s_1} \neq \mathbf{c}_{s_2}$. In other words, $\mathcal{E}_{\mathbb{F}_2} : \mathcal{S} \rightarrow \mathcal{I}_S$ is injective (one-to-one). Consequently, if we define the function $\mathcal{D}_{\mathbb{F}_2}$ over \mathcal{I}_S as the inverse function of $\mathcal{E}_{\mathbb{F}_2}$, i.e., $\mathcal{E}_{\mathbb{F}_2}^{-1} \triangleq \mathcal{D}_{\mathbb{F}_2} : \mathcal{I}_S \rightarrow \mathcal{S}$, then we have that $\hat{\mathbf{s}} = \mathcal{D}_{\mathbb{F}_2}(\mathcal{E}_{\mathbb{F}_2}(\mathbf{s})) = \mathbf{s}, \forall \mathbf{s} \in \mathcal{S}$.

B. MmWave Beam Discovery

Let $\mathbf{q}^a \in \mathbb{C}^{n_r}$ denote the angular **channel vector** between TX and RX. Define $\mathbf{q}_s^a \in \{0, 1\}^{n_r}$ to be the **support vector** associated with \mathbf{q}^a such that

$$\mathbf{q}_s^a = \begin{pmatrix} q_{s_1}^a \\ q_{s_2}^a \\ \vdots \\ q_{s_{n_r}}^a \end{pmatrix}, \quad \text{where } q_{s_i}^a = \begin{cases} 1, & \text{if } q_i^a \neq 0 \\ 0, & \text{if } q_i^a = 0 \end{cases} \quad (16)$$

More generally, a support vector can be defined as:

Definition V.2 (Support vector). The support vector \mathbf{v}_s associated with an arbitrary n -dimensional vector $\mathbf{v} \in \mathbb{C}^n$ is a binary vector of the same size that identifies the non-zero components of \mathbf{v} and whose components, v_{s_i} , are defined as

$$v_{s_i} = \begin{cases} 1, & v_i \neq 0 \\ 0, & v_i = 0 \end{cases} \quad (17)$$

We further define the set of non-zero indexes \mathcal{X}_v of an arbitrary vector \mathbf{v} as follows:

Definition V.3 (Set of Non-Zero Indexes \mathcal{X}_v). For any arbitrary n -dimensional vector \mathbf{v} , we define \mathcal{X}_v as the set of indexes of its non-zero components, i.e.,

$$\mathcal{X}_v = \{i | v_i \neq 0, 0 \leq i \leq n-1\} \quad (18)$$

Hence, if \mathbf{v}_s is the support vector corresponding to \mathbf{v} , then we have that $\mathcal{X}_v = \mathcal{X}_{\mathbf{v}_s}$, since $v_i = 0 \iff v_{s_i} = 0$.

Now, let \mathcal{Q}^a be the set containing all possible channel vectors \mathbf{q}^a . Also let \mathcal{Q}_s^a be the set of all support vectors \mathbf{q}_s^a such that their corresponding channels $\mathbf{q}^a \in \mathcal{Q}^a$. An interesting behavior we have for these sets is as follows: If we have a channel \mathbf{q}_1^a whose support vector $\mathbf{q}_{s_1}^a \in \mathcal{Q}_s^a$, then removing any non-zero component(s) from \mathbf{q}_1^a (due to blockage for example) would still yield a valid channel $\mathbf{q}_2^a \in \mathcal{Q}^a$, whose support vectors $\mathbf{q}_{s_2}^a$ also belongs to \mathcal{Q}_s^a . We call this the **inclusion property**.

Definition V.4. [Inclusion Properties of \mathcal{Q}_s^a]

- (i) Let $\mathbf{q}_{s_1}^a, \mathbf{q}_{s_2}^a \in \{0, 1\}^{n_r}$ such that $\mathcal{X}_{\mathbf{q}_{s_2}^a} \subseteq \mathcal{X}_{\mathbf{q}_{s_1}^a}$. If $\mathbf{q}_{s_1}^a \in \mathcal{Q}_s^a$, then $\mathbf{q}_{s_2}^a \in \mathcal{Q}_s^a$.
- (ii) $\mathbf{0} \in \mathcal{Q}_s^a$. In fact, this is a consequence of property (i) above since for any $\mathbf{q}_s^a \in \mathcal{Q}_s^a$, we have that $\mathcal{X}_{\mathbf{0}} = \emptyset \subseteq \mathcal{X}_{\mathbf{q}_s^a}$.

Now, we are ready to present the theorem that establishes the conditions that need to be satisfied by a linear source code so that each possible channel \mathbf{q}^a would result in a **unique** measurement vector \mathbf{y}^s . Impairments under noise are not addressed in this theorem.

Theorem 1. Consider a binary linear source code \mathcal{C} whose encoding function \mathcal{E} (defined by the binary generator matrix \mathbf{G}) is an injective function defined over $\mathcal{Q}_s^a \in \{0, 1\}^{n_r}$. If we consider \mathbf{G} to be defined over the complex field, then for all channel vectors $\mathbf{q}_1^a, \mathbf{q}_2^a \in \mathcal{Q}^a \subseteq \mathbb{C}^{n_r}$ we have $\mathbf{q}_1^a \neq \mathbf{q}_2^a$ if and only if $\mathbf{G}\mathbf{q}_1^a = \mathbf{y}_1^s \neq \mathbf{y}_2^s = \mathbf{G}\mathbf{q}_2^a$.

Proof. Let $\mathbf{q}_1^a, \mathbf{q}_2^a \in \mathcal{Q}^a$, and let $\mathbf{y}_i^s = \mathbf{G}\mathbf{q}_i^a$. Now, assume that

$\mathbf{q}_1^a \neq \mathbf{q}_2^a$. Then, we have that

$$\mathbf{y}_1^s - \mathbf{y}_2^s = \mathbf{G}\mathbf{q}_1^a - \mathbf{G}\mathbf{q}_2^a = \mathbf{G}(\underbrace{\mathbf{q}_1^a - \mathbf{q}_2^a}_{=\mathbf{v}}) = \mathbf{G}\mathbf{v} \quad (19)$$

$$= \sum_{i=1}^{n_r} v_i \times \mathbf{g}_i = \sum_{i \in \mathcal{X}_v} v_i \times \mathbf{g}_i \quad (20)$$

where \mathbf{g}_i is the i^{th} column of \mathbf{G} .

To show that $\mathbf{y}_1^s - \mathbf{y}_2^s \neq \mathbf{0}$, we need to show that all vectors $\mathbf{g}_i \forall i \in \mathcal{X}_v$, are linearly independent. Otherwise, if such vectors \mathbf{g}_i are linearly **dependent**, then $\exists v_i \in \mathbb{R}$ for $i \in \mathcal{X}_v$ such that $\mathbf{y}_1^s - \mathbf{y}_2^s = \mathbf{G}\mathbf{v} = \mathbf{0}$.

In fact, we can show a stronger statement: “all vectors $\mathbf{g}_i \forall i \in \mathcal{X}_{\mathbf{q}_1^a} \cup \mathcal{X}_{\mathbf{q}_2^a} \supseteq \mathcal{X}_v$, are linearly independent”. Note that $\mathcal{X}_{\mathbf{q}_1^a}$ and $\mathcal{X}_{\mathbf{q}_2^a}$ are the sets of indexes of the non-zero components of \mathbf{q}_1^a and \mathbf{q}_2^a , respectively (recall Definition V.3) and that $\mathcal{X}_{\mathbf{q}_1^a} = \mathcal{X}_{\mathbf{q}_{s_1}^a}$ and $\mathcal{X}_{\mathbf{q}_2^a} = \mathcal{X}_{\mathbf{q}_{s_2}^a}$.

- First, let us show that \mathcal{X}_v is a subset of $\mathcal{X}_{\mathbf{q}_1^a} \cup \mathcal{X}_{\mathbf{q}_2^a}$. Since $v_i = q_{1,i}^a - q_{2,i}^a \forall 1 \leq i \leq n_r$, then $q_{1,i}^a = q_{2,i}^a = 0 \implies v_i = 0$. Therefore, we have

$$\mathcal{X}_{\mathbf{q}_1^a}^c \cap \mathcal{X}_{\mathbf{q}_2^a}^c = \{\mathcal{X}_{\mathbf{q}_1^a} \cup \mathcal{X}_{\mathbf{q}_2^a}\}^c \subseteq \mathcal{X}_v^c \quad (21)$$

Then, by taking the complements of both sides we obtain the required result (note that $\{\cdot\}^c$ denotes a set complement).

- Second, we show that vectors in the set $\mathcal{G} \triangleq \{\mathbf{g}_i | i \in \mathcal{X}_{\mathbf{q}_1^a} \cup \mathcal{X}_{\mathbf{q}_2^a}\}$ are linearly independent over \mathbb{F}_2 : Assume towards contradiction that \mathcal{G} is linearly dependent over \mathbb{F}_2 . Hence, there exists a set $\mathcal{G}_D \subseteq \mathcal{G}$ such that any $\mathbf{g}_{i_0} \in \mathcal{G}_D$ can be written as a linear combination of all other vectors in \mathcal{G}_D , i.e.,

$$\mathbf{g}_{i_0} = \sum_{\substack{j: j \neq i_0 \\ \mathbf{g}_j \in \mathcal{G}_D}} \mathbf{g}_j \pmod{2}. \quad (22)$$

Note that over \mathbb{F}_2 , we can assume, without loss of generality (W.L.O.G.), that the coefficients of the linear combination above are 1's. Hence, we have that

$$\sum_{j: \mathbf{g}_j \in \mathcal{G}_D} \mathbf{g}_j \pmod{2} = \mathbf{0} \quad (23)$$

Next, assume that $\exists \mathbf{q}_{s_3}^a, \mathbf{q}_{s_4}^a \in \mathcal{Q}_s^a$ such that $\mathcal{X}_{\mathbf{v}_s} = \{j | \mathbf{g}_j \in \mathcal{G}_D\}$ where $\mathbf{v}_s = \mathbf{q}_{s_3}^a - \mathbf{q}_{s_4}^a \pmod{2}$. Then, since \mathbf{G} is injective over \mathcal{Q}_s^a , then we have that

$$\mathbf{G}\mathbf{v}_s \pmod{2} = \sum_{j \in \mathcal{X}_{\mathbf{v}_s}} \mathbf{g}_j \pmod{2} = \sum_{j: \mathbf{g}_j \in \mathcal{G}_D} \mathbf{g}_j \pmod{2} \quad (24)$$

$$\neq \mathbf{0} \xleftrightarrow{\text{iff}} \mathbf{v}_s \pmod{2} \neq \mathbf{0} \quad (25)$$

But, if \mathcal{G}_D is non-empty, then $\mathbf{v}_s \neq \mathbf{0}$. Hence, we arrive at a contradiction to Eq. (22). Therefore, the set \mathcal{G} is linearly independent over $GF(2)$.

It remains to show that such $\mathbf{q}_{s_3}^a$ and $\mathbf{q}_{s_4}^a$ indeed exist.

Let us construct $\mathbf{q}_{s_3}^a$ as follows:

First, let $\mathbf{q}_{s_3}^a = \mathbf{q}_{s_1}^a$, then, reset its i^{th} component to 0 ($q_{s_3,i}^a = 0$) if $\mathbf{g}_i \notin \mathcal{G}_D$. Similarly, set $\mathbf{q}_{s_4}^a = \mathbf{q}_{s_2}^a$, then, reset the i^{th} component to 0 ($q_{s_4,i}^a = 0$) if $\mathbf{g}_i \notin \mathcal{G}_D$ OR if $q_{s_1,i}^a = 1$.

Then, by construction, we have $\mathcal{X}_{\mathbf{q}_{s_3}^a} \subseteq \mathcal{X}_{\mathbf{q}_{s_1}^a}$ and $\mathcal{X}_{\mathbf{q}_{s_4}^a} \subseteq \mathcal{X}_{\mathbf{q}_{s_2}^a}$. Hence, by the inclusion property (recall remark V.4) we have $\mathbf{q}_{s_3}^a, \mathbf{q}_{s_4}^a \in \mathcal{Q}_s^a$ since both

$\mathbf{q}_{s_1}^a, \mathbf{q}_{s_2}^a \in \mathcal{Q}_s^a$. Also, it is easy to see that $q_{s_3,j}^a - q_{s_4,j}^a \pmod 2 = 1 \forall j : \mathbf{g}_j \in \mathcal{G}_D$.

- Third, by Lemma 2 below, the set \mathcal{G} , now taken over \mathbb{R} , is linearly independent.

Therefore, in Eq. (20), it follows that $\mathbf{y}_1^s - \mathbf{y}_2^s \neq \mathbf{0}$ if and only if $\mathbf{q}_1^a - \mathbf{q}_2^a \neq \mathbf{0}$, which concludes the proof. \square

Lemma 2 . Any set of n -dimensional linearly independent vectors over \mathbb{F}_2 are also linearly independent over \mathbb{C} if we interpret their $0_{\mathbb{F}_2}$ and $1_{\mathbb{F}_2}$ components to be real scalars.

The proof is provided in Appendix A.

C. On the lower bound on the number of measurements

In Theorem 1, we showed that a linear source code C which can **uniquely** encode all $\mathbf{q}_s^a \in \mathcal{Q}_s^a$ can be used to design a framework that uniquely measures all $\mathbf{q}^a \in \mathcal{Q}^a$. Let the compression ratio of the code C be denoted by r_c such that

$$r_c = \frac{m}{n_r} \quad (26)$$

where m and n_r are the number of rows and columns of C 's generator matrix \mathbf{G} , respectively.

Reducing the number of measurements is a fundamental objective for the mm-wave beam discovery problem. In light of Theorem 1, we can see that finding a source code with a high compression rate (small r_c) is crucial for attaining such an objective. In the following discussion, we try to better understand the nature of this lower bound in the context of our proposed solution.

Corollary 2.1 . Let \underline{m} denote the lowest possible number of measurements for mm-wave beam discovery using lossless, fixed-rate source coding. Then, we have

$$\underline{m} \geq \left\lceil \log_2 \left(\sum_{i=0}^L \binom{n_r}{i} \right) \right\rceil \geq H_2(\mathbf{q}_s^a) \quad (27)$$

where $H_2(\cdot)$ is the binary entropy function.

Proof. Suppose that C is a linear lossless fixed-rate source code which can uniquely compress all $\mathbf{q}_s^a \in \mathcal{Q}_s^a$. By Theorem 1, we have that the number of measurements needed for estimating the mm-wave channel is equal to m (the length of encoded channel support vectors). Since the length of compressed sequences for any such code is lower bounded by $H_2(\mathbf{q}_s^a)$, then we have $\underline{m} \geq H_2(\mathbf{q}_s^a)$. Moreover, since fixed-rate source codes do not take the probability distribution (i.e., frequency) of \mathbf{q}_s^a into account, then we have

$$\underline{m} \geq \sup_{\mathbb{P}(\mathbf{q}_s^a)} H_2(\mathbf{q}_s^a) \geq H_2(\mathbf{q}_s^a), \text{ where} \quad (28)$$

$$\sup_{\mathbb{P}(\mathbf{q}_s^a)} \sum_{\mathbf{q}_s^a \in \mathcal{Q}_s^a} \mathbb{P}(\mathbf{q}_s^a) \log_2 \left(\frac{1}{\mathbb{P}(\mathbf{q}_s^a)} \right) = \log_2(|\mathcal{Q}_s^a|) \quad (29)$$

The result of solving the sup problem in Eq. (29) is $\mathbb{P}(\mathbf{q}_s^a) = \frac{1}{|\mathcal{Q}_s^a|} \forall \mathbf{q}_s^a$ since the uniform distribution maximizes the entropy. Since the number of measurement has to be an integer, we take the ceil of right hand side of Eq. (29). Finally, by the inclusion property in Definition V.4, we have $|\mathcal{Q}_s^a| = \sum_{i=0}^L \binom{n_r}{i}$, which concludes the proof. \square

D. Channel Estimation Error

In Theorem 1, we have shown how to obtain unique measurements $\mathbf{y}^s \forall \mathbf{q}^a \in \mathcal{Q}^a$. We did not, however, discuss the effect of errors that occur during channel measurements. Recall that the source of measurement errors include **channel noise** and **quantization**. The quality of channel estimates we obtain based on error-corrupted measurements is essentially degraded, which calls for a deeper understanding of the effects of such errors. An interesting question we try to answer here is: **Do small perturbations/imperfections in channel measurements make channel estimates considerably deviate from their true values?** In this section, we shed some light on this problem by deriving an upper bound on channel estimation error as a function of measurement error. We also show that for a special class of generator matrices, the channel estimation error, measured using the l_2 -norm, is smaller than that of the measurement error vector.

We denote error-corrupted measurements using \mathbf{u}^s such that

$$\mathbf{u}^s = \mathbf{y}^s + \mathbf{z} \quad (30)$$

where \mathbf{z} is the measurement error (recall Eq. (13) and the discussion that follows). Let us assume that we can **perfectly** decode any measurement vector into its corresponding channel vector. In other words, for any measurement vector \mathbf{y}^s , we can find its corresponding channel \mathbf{q}^a such that $\mathbf{y}^s = \mathbf{G}\mathbf{q}^a$ (measurement decoding will be further discussed in Section VI). Let us also denote the *channel estimate* we obtain based on the error-corrupted measurement \mathbf{u}^s by $\hat{\mathbf{q}}^a$, i.e., $\mathbf{u}^s = \mathbf{G}\hat{\mathbf{q}}^a$. The following proposition provides an upper bound on the channel estimation error in terms of measurements errors.

Proposition 3 . Assuming perfect decoding of channel measurements, the channel estimation error is upper bounded as:

$$\|\hat{\mathbf{q}}^a - \mathbf{q}^a\|_2 \leq \frac{1}{\sigma_{\min}(\mathbf{G})} \|\mathbf{z}\|_2 \quad (31)$$

where $\sigma_{\min}(\cdot)$ is the minimum singular value of a given matrix.

Proof. Let us start by writing \mathbf{z} as

$$\mathbf{z} = \mathbf{u}^s - \mathbf{y}^s = \mathbf{G}(\hat{\mathbf{q}}^a - \mathbf{q}^a) \quad (32)$$

$$\implies \|\mathbf{z}\|_2 = \|\mathbf{G}(\hat{\mathbf{q}}^a - \mathbf{q}^a)\|_2 \quad (33)$$

$$= \|(\hat{\mathbf{q}}^a - \mathbf{q}^a)\|_2 \times \frac{\|\mathbf{G}(\hat{\mathbf{q}}^a - \mathbf{q}^a)\|_2}{\|(\hat{\mathbf{q}}^a - \mathbf{q}^a)\|_2} \quad (34)$$

$$\geq \|(\hat{\mathbf{q}}^a - \mathbf{q}^a)\|_2 \times \sigma_{\min}(\mathbf{G}) \quad (35)$$

Finally, by rearranging (35), we obtain the required statement

$$\|\hat{\mathbf{q}}^a - \mathbf{q}^a\|_2 \leq \frac{1}{\sigma_{\min}(\mathbf{G})} \|\mathbf{z}\|_2 \quad \square$$

Now, we see that if $\sigma_{\min}(\mathbf{G}) \geq 1$, then the channel estimation error (measured using the l_2 -norm) is smaller than or equal to the l_2 -norm of the measurement error, i.e., $\|\hat{\mathbf{q}}^a - \mathbf{q}^a\|_2 \leq \|\mathbf{z}\|_2$. This, in fact, is the case for the class of generator matrices introduced in the following proposition

Proposition 4 . For generator matrices in the form:

$$\mathbf{G} = (\mathbf{I}_m \mid \mathbf{P}_{m \times n-m}) \quad (36)$$

where \mathbf{I}_m is the $m \times m$ identity matrix, we have $\sigma_{\min}(\mathbf{G}) \geq 1$.

See Appendix C for proof.

Remark. It is not difficult to obtain generator matrices of the form in Eq. (36). For instance, syndrome source codes can be manipulated using row and column operations over the binary field to produce equivalent codes with \mathbf{G} as in Eq. (36).

VI. MEASUREMENT DECODING

Designing channel measurements that have one-to-one correspondence with \mathbf{q}^a is only part of the solution. Equally important, however, is the ability to “decode” \mathbf{y}^s back to \mathbf{q}^a , i.e., figuring out the function $\mathcal{D}(\cdot)$ in Eq. (14c). The one-to-one correspondence between \mathbf{q}^a and \mathbf{y}^s guarantees that there exists an inverse function that maps \mathbf{y}^s back to \mathbf{q}^a . Nevertheless, since we can only obtain \mathbf{u}^s ; an error-corrupted version of \mathbf{y}^s , we cannot exactly regenerate \mathbf{q}^a , but rather, an estimate $\hat{\mathbf{q}}^a$. Given that measurement errors occur, our objective is to obtain $\hat{\mathbf{q}}^a$ such that its *distance* to \mathbf{q}^a is as small as possible (i.e., minimize the estimation error). We use the l_2 -norm as a distance measure between \mathbf{q}^a and $\hat{\mathbf{q}}^a$, defined as:

$$\delta(\mathbf{q}^a, \hat{\mathbf{q}}^a) = \|\mathbf{q}^a - \hat{\mathbf{q}}^a\|_2 = \sqrt{\sum_{i=0}^{n_r-1} (q_i^a - \hat{q}_i^a)^2} \quad (37)$$

The problem of mapping the channel measurements to an estimated channel is non-linear and may require intensive computations. Two different methods to do this mapping were proposed in [18], namely, i) the “look-up table” method and ii) the “search” method. The look-up table method requires storing a table with entries for all possible channel measurements along with their corresponding channels. This is possible since measurements are quantized using ADCs and hence there exists a finite number of possibilities for \mathbf{y}^s . However, the number of entries in the table could be quite large, especially, if high resolution ADCs are used. On the other hand, the search method requires a combinatorial search over the columns of \mathbf{G} (recall that $\mathbf{y}^s \equiv \mathbf{G}\mathbf{q}^a$) for which the computational complexity is of order $O(n_r^L)$. This could be prohibitive for large antenna arrays. Motivated by the drawbacks of the look-up table and search methods, we propose an alternative *Machine Learning (ML)* based approach that uses *Deep Neural Networks (DNN)*.

A. DNN-based mapping

ML is widely used to solve very complex problems through *learning*. We focus on *supervised learning* to solve the decoding problem, which is a multi-dimensional non-linear regression problem for which neural networks is a powerful tool. Specifically, we use a fully connected classical DNN with an input layer of m nodes (equal to the measurement dimension) and an output layer of n_r nodes (equal to the channel dimensions). That is, the DNN takes the measurement vectors \mathbf{y}^s as an input and produces the corresponding channel estimate $\hat{\mathbf{q}}^a$ at its output. The number of hidden layers and their corresponding number of nodes are design parameters that depend on the sizes of the input and output, and the relationship governing them. For all hidden layers, we use the rectified linear (ReLU) activation function while for the output layer we use the linear activation function. We also use

the *ADAM* optimizer [30] for training and the Mean Squared Error (MSE) loss function to quantify the model error².

Model training: Although we do not have a closed form expression for mapping \mathbf{y}^s to \mathbf{q}^a (hence the need for an algorithmic solution), generating training data is actually straightforward. This is because the reverse direction (i.e., mapping \mathbf{q}^a to \mathbf{y}^s) is just a simple linear transformation. Training data is generated as follows: For every $\mathbf{q}_s^a \in \mathcal{Q}_s^a$ (recall that \mathcal{Q}_s^a is the set of all possible channel support vectors defined in Section V-B), we generate $n_s = 300$ random channels \mathbf{q}^a by choosing the non-zero components of \mathbf{q}^a to be uniformly distributed in $[-\alpha_{\max}^b, \alpha_{\max}^b]$ where α_{\max}^b is the maximum magnitude of expected baseband path gains which can be obtained using channel statistics (recall Eq. (5)). Thus, the total number of input-output samples we have is $n_s \times |\mathcal{Q}_s^a|$. We use 70% of these samples for training and the remaining 30% for validation. Training is done using 200 epochs with batches of size 32. We monitor the validation error to make sure that the model does not over-fit the training data. If overfitting is observed (which is indicated by a persistent increase in validation error at the end of every epoch), we stop the training process and only keep the model which produced the least validation error.

B. DNN Model Assessment

To argue the reliability of DNN-based mapping, we test it using channel with $n_t=1$, $n_r=23$ and a maximum of 3 paths i.e., $L \leq 3$. We also compare the DNN model performance to the “search” method of [18]. Based on the described channel parameters, only $m=11$ measurements are needed to discover its paths (more details about this particular example are discussed in Section VIII). We design a DNN model with an input layer of $m=11$ nodes and an output layer of $n_r=23$ nodes. The model also has 5 hidden layers with 1024, 512, 512, 128 and 128 nodes, respectively. We train the DNN model using data generated as described in Section VI-A. Fig. 4a shows the average MSE loss of both training and validation data sets for 100 epochs. The trained model achieves an average validation error of ≈ 0.0143 (averaged across all samples of validation data). The figure also shows close MSE values for training and validation. This indicates that the model generalizes well to measurements it had not seen before, which guarantees its reliability for arbitrary future measurements.

These initial results are promising. However, they are obtained using error-free measurements. This prompts us to test the resilience of DNN-based mapping against noisy measurements. We also compare its performance against the search method proposed in [18]. To do so, we generate a testing data set in the same way we created the training data. We also generate sets of uniformly distributed noise vectors where each noise set is drawn at a different value of transmit SNR from -20 to 20 dB. The noise vectors are then added to the inputs (channel measurements) of the testing data set then passed through the trained model. The decoded $\hat{\mathbf{q}}^a$ is recorded at the

²We use Keras API [31] to build, train, test and use the DNN model we propose. Our pre-trained models and DNN-related codes are available in [32].

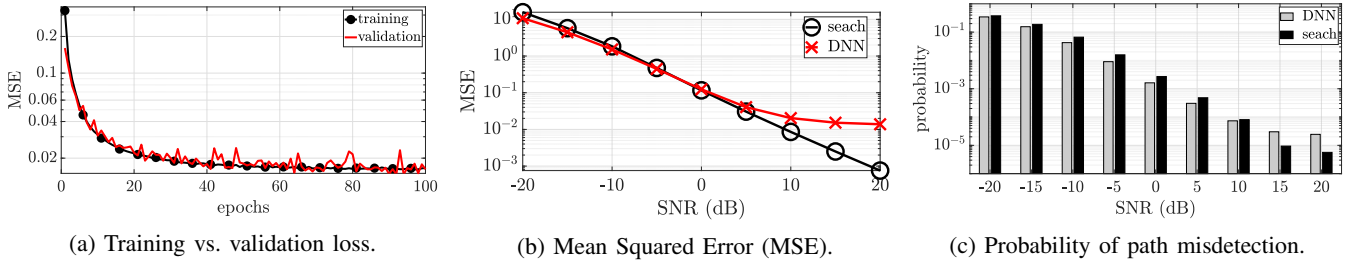


Fig. 4: Evaluation of DNN-based measurement to channel mapping.

output. Similarly, we use the “search” method to decode the same noise-corrupted measurements.

For evaluation, we use i) the average MSE, as well as ii) the probability of path misdetection (i.e., no path discovery). We say a path is correctly discovered if the path gain of its corresponding component in \hat{q}^a is among the $L=3$ strongest components in \hat{q}^a . Fig. 4b shows the average MSE obtained using the search and DNN-based mapping methods on a log scale. We see that at low SNR, DNN-based decoding outperforms the search method. This indicates that the DNN model is more resilient against measurement errors. At high SNR, however, the DNN’s MSE saturates at ≈ 0.014 which is the same value we obtain for validation during model training using noise-free inputs³. The search method’s MSE, on the other hand, keeps improving as SNR increases, nevertheless, for values below 10^{-2} the improvement is marginal. The probability of path misdetection, shown in Fig. 4c, confirms the performance trend of the MSE. Specifically, we see that at low SNR, the DNN-based model outperforms the search method (i.e., has lower probability of misdetection) while at high SNR we see that the search method is better.

Computational complexity: As we have previously discussed, the search method requires high computational power. Precisely, $\binom{n_r}{L}$ iterations with one matrix inversion and two matrix multiplication operations are performed per iteration, which then produces a vector of length m . Finally, an additional step of finding the minimum l_2 -norm of all $\binom{n_r}{L}$ vectors is performed. On the other hand, the DNN-based mapping just requires N_k linear computations for the hidden and output layers, where N_k is the number of nodes at the k^{th} layer. These computations are of the form $\sum_{i=1}^{N_{k-1}} w_i a_i$ where a_i is the value passed from the i^{th} node of the previous layer and w_i is the weight on its link. For this particular example, the search method and the DNN-based method were implemented on the same machine and on average the search method’s execution time was 11.2 ms compared to 47 μ s for the DNN model.

VII. MULTIPLE TRANSMIT AND RECEIVE ANTENNAS

Up to this point, we have only dealt with channels with single-transmit, multiple-receive antennas. Recall that this setting is almost identical to that of multiple-transmit, single-receive antennas. The difference is that in the former setting we seek to design w_i ’s to estimate the angular channel at RX,

while in the latter, we design f_j ’s in order to estimate the angular channel at TX. In this section, we extend the channel setting to be of **multiple-transmit, multiple-receive** antennas. We show how measurements are obtained and decoded to estimate the entire $n_r \times n_t$ channel. This is achieved by building on the design principles and decoding methods of single transmit antenna channels.

A. Measurements

Unlike the single transmit antenna scenario where TX sends signals omnidirectionally, it can now focus its transmission on narrow angular directions. However, from RX’s point of view, no matter which set of directions the TX is transmitting into, it can only see a number of n_r resolvable bins; only L of which may have paths to TX. The same is true from TX’s perspective, where the TX can only see n_t resolvable bins, only L of which may have paths to the receiver⁴. Thus, for an arbitrary tx-precoder, the receiver would need to measure the channel using the same set of w_i ’s it needs for the $n_t = 1$ setting. Upon decoding, the result would be n_r angular rx bins (corresponding to the particular f_j used at TX). Similarly, for an arbitrary rx-combiner, the transmitter would need the same set of f_j ’s it needs for the $n_r = 1$ setting to find its respective tx bins. To find such f_j ’s and w_i ’s, we invoke Theorem 1.

Let $f_j \forall j \in \{1, \dots, m_t\}$ be the tx-precoding vectors and $w_i \forall i \in \{1, \dots, m_r\}$ be the rx-combining vectors. Then, the channel measurements are obtained as follows: The transmitter sends a number of m_r pilot symbols using **each** of its m_t precoders. On the receiver side, for every tx-precoder, m_r channel measurements are obtained using the distinct m_r rx-combiners. Recall that $u_{i,j} = y_{i,j}^s + w_i^H n$ where $y_{i,j}^s = w_i^H Q f_j$ (see Eq. (12)). Let us arrange the m_r measurements corresponding to the j^{th} tx-precoder in y_j^s and define Y^s as

$$Y^s \triangleq \begin{pmatrix} y_1^s & y_2^s & \dots & y_{m_t}^s \end{pmatrix} \quad (38)$$

Thus, Y^s contains all $m_t \times m_r$ channel measurements necessary to discover all available paths.

B. Decoding Y^s

To obtain \hat{Q}^a from Y^s , we perform multiple SIMO decoding operations as described in Section VI. This procedure is highlighted in the diagram shown in Fig. 5 and is detailed as follows:

³The MSE value at which DNN-based mapping saturates can be made lower by further improvement of the DNN model.

⁴Recall that the directions at which the TX is transmitting and the RX is receiving are determined by their antenna beam patterns which are in turn determined by f_j and w_i , respectively (see Fig. 2).

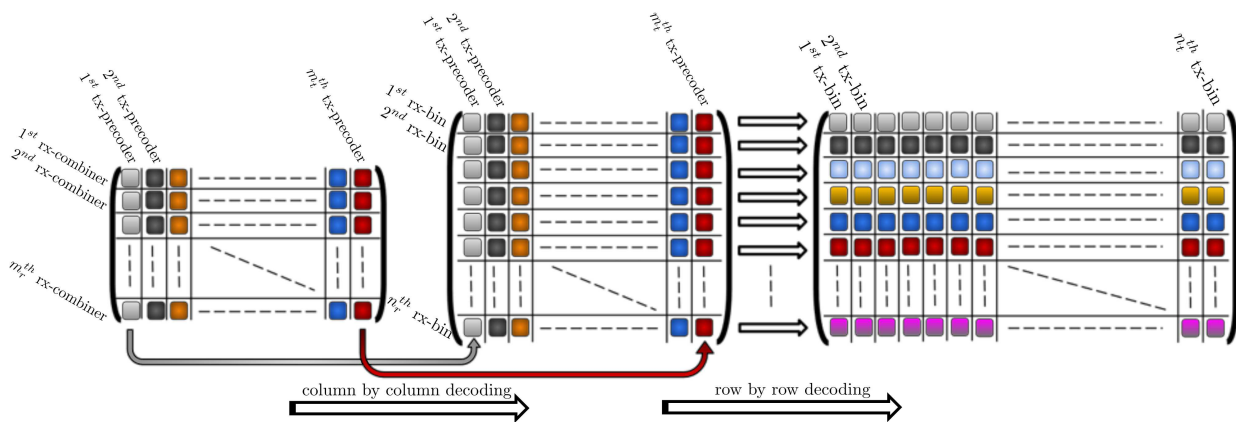


Fig. 5: Measurement decoding for channels with multiple TX/RX antennas is done in two steps. Given the matrix \mathbf{Y}^s whose $y_{i,j}^s$ th component is $= \mathbf{w}_i^H \mathbf{Q} \mathbf{f}_j$ (shown on the left), we first do a column by column decoding where the j^{th} decoded column of \mathbf{Y}^s is $\mathbf{q}_{rx,j}^a$. Then, in the second step we decode the intermediary matrix row by row to produce $\hat{\mathbf{Q}}^a$ (shown on the right). The two decoding functions of first and second steps are dependent on the source codes used to design \mathbf{w}_i 's and \mathbf{f}_j 's, respectively.

- (i) Decode every $\mathbf{y}_j^s \forall j \{1, 2, \dots, m_t\}$ to obtain $\mathbf{q}_{rx,j}^a$. Recall that \mathbf{y}_j^s is the measurement vector corresponding to the j^{th} tx-precoder. Thus, $\mathbf{q}_{rx,j}^a$ is the $n_r \times 1$ mm-wave channel observed at RX due to the TX signal transmission through the angular directions featured by \mathbf{f}_j .
- (ii) After Step (i), we obtain a sequence of m_t “measurement” components corresponding to each rx-bin. Each of these components is produced using a distinct tx-precoder. Let us denote these sequences by $\mathbf{y}_{tx,k}^s$ ($1 \times m_t$ row vectors), where $k \in \{1, 2, \dots, n_r\}$.
- (iii) Decode each $\mathbf{y}_{tx,k}^s$ to obtain $\mathbf{q}_{tx,k}^a$ ($1 \times n_t$ row vectors) whose components constitute all the tx-bins corresponding to the k^{th} rx-bin.
- (iv) Stack all $\mathbf{q}_{tx,k}^a$ to obtain $\hat{\mathbf{Q}}^a$ (each representing the k^{th} row of $\hat{\mathbf{Q}}^a$).

VIII. PERFORMANCE EVALUATION

We provide two different simulation scenarios⁵. The first one is for mm-wave channels with $n_t = n_r = 23$ antennas, and a maximum number of $L=3$ paths (note that L can be obtained from statistical channel models [3], [34]). For this scenario, we consider various finite ADC resolutions as well as the ideal, infinite resolution setting. This highlights the effect of ADC resolution on performance. We also use this scenario to compare various measurement decoding methods. Specifically, our proposed DNN-based decoding with and without noise defense (explained in Section VIII-C), as well as the search method of [18]. The second scenario is for *single-path* channels ($L=1$) with $n_t=31$ and $n_r=15$. We use this scenario to evaluate our proposed method against CS based methods and the beam alignment scheme of the IEEE 802.11ad standard. We opt for single-path channels for this comparison since 802.11ad can only find one channel path⁶.

⁵ We used tensorflow [33] for creating and using DNN models.

⁶ Channels with one path can be assumed if we only wish to find the LoS path. This is valid since the path loss of Non-LoS paths is approximately 20 dB higher than that of LoS [3], hence they could be neglected.

A. Performance Metrics

We adopt performance metrics that highlight: (i) the measurement overhead, (ii) accuracy of path discovery and (iii) quality of the estimated path gains. These metrics are evaluated numerically, using Monte Carlo simulations (averaged over 10^5 simulation runs) and evaluated against different values of SNR. We define the performance metrics as follows:

- i) Number of measurements:* Given by $m_t \times m_r$.
- ii) Probability of path discovery:* Paths are said to exist at the strongest L components in the estimated channel $\hat{\mathbf{Q}}^a$.
- iii) MSE:* Defined as the Frobenius norm $\|\mathbf{Q}^a - \hat{\mathbf{Q}}^a\|_F$.

B. Choice of linear source codes

Recall from our discussion in Section VII that we design \mathbf{f}_j 's and \mathbf{w}_i 's for $n_r \times n_t$ channels using the same \mathbf{f}_j 's used for $1 \times n_t$ channels and the \mathbf{w}_i 's used for $n_r \times 1$ channels. In both cases, we invoke Theorem 1 which states that the chosen source codes should uniquely encode all support vectors. Based on this criterion, we choose the codes as follows:

- 1) *Multi-path channel with $n_r = n_t = 23$ and $L \leq 3$:* For this channel, since $n_r = n_t$, the same source code works for designing both tx-precoders and rx-combiners. Thus, we need to find a code whose encoding function \mathcal{E} is injective over the set of support vectors representing all possible TX (and RX) bins. The *perfect binary Golay code* used as a syndrome source code is a suitable choice for this problem. This code also achieves the binary entropy if all support vectors of the tx/rx bins have the same probability of occurrence. It has a generator matrix of size 11×22 , hence, we have $m_t = m_r = 11$, and the total number of required channel measurements is $m_t \times m_r = 121$. Compared to the exhaustive search approach, which requires scanning all combinations of TX/RX angular directions, this represents **75%** measurement reduction.

- 2) *Single-path channel with $n_t = 31, n_r = 15$ and $L \leq 1$:* Since $n_t \neq n_r$, we need to choose different codes to design the tx-precoders and rx-combiners. At the TX side, we can choose the (31, 26) Hamming code while at the RX side we choose the (15, 11) Hamming code, both of which operate as

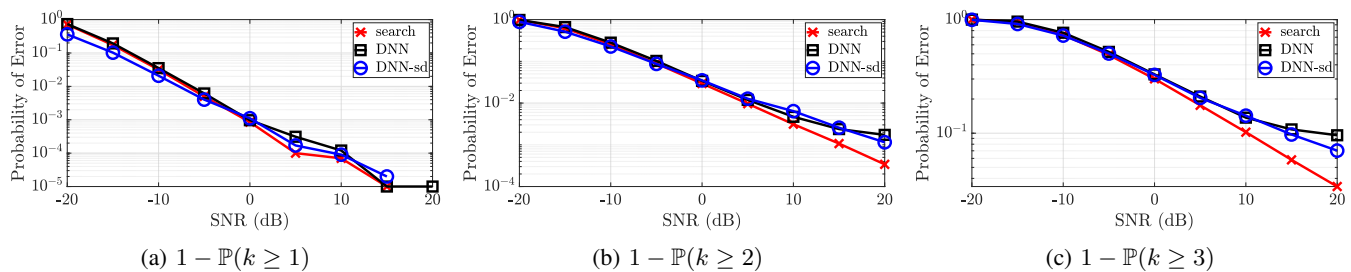


Fig. 6: Beam detection probability for infinite resolution ADCs.

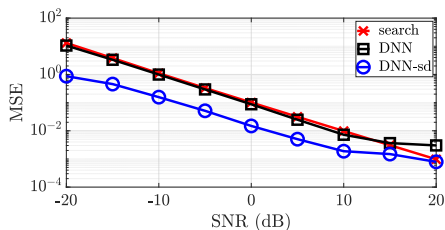


Fig. 7: MSE for infinite resolution ADCs.

syndrome source codes with generator matrices \mathbf{G}_t and \mathbf{G}_r of sizes 5×31 and 4×15 , respectively. Hence, we have $m_t=5$ and $m_r=4$, which gives us a total number of 20 measurements. On the other hand, the exhaustive search approach requires 465 measurements (95% reduction), while the IEEE 802.11ad scheme requires 46 measurements (57% reduction).

C. DNN model design and training

We design DNNs to have 3 hidden layers, with 6000, 1000 and 250 nodes (neurons) for each layer, respectively. This provides a reasonably good input-to-output mapping performance while keeping the processing speed fairly fast. Two types of DNN training are considered. The first type is *error-free* training where the training examples are pure, with no added noise components. This is similar to the approach taken in Section VI-B. Measurement errors, however, tend to degrade the performance of path discovery. One way to overcome this impediment is by augmenting the training data with noise to prevent over-fitting. This provides the DNN model with defense against error corrupted measurements. It represents the second type of training which will be shown to further enhance the performance of beam discovery.

D. 23×23 Multipath Channel Results

In this section, we present the simulation results for 23×23 channels with $L \leq 3$. We divide our discussion into two parts. In the first part, we provide the results for systems with infinite resolution ADCs. While impractical, assuming ideal ADCs can help us understand the upper bound of performance for our proposed beam discovery solution. It also gives an insight into how much resolution is needed to take full advantage of our proposed scheme. Results for finite resolution ADCs are provided in the second part of the discussion, where the desired ADC resolution is shown to be dependent on SNR.

1) *Infinite Resolution ADC*: We present the performance of beam discovery using both “search” and “DNN-based” measurement decoding. For the DNN-based method, we present two categories of models: the first category is for models trained using error-free measurements, which can be used at all values of transmit SNR, while the second category is for specially trained DNN models with defense against specific noise power values. In other words, the latter category requires a separate DNN model for each level of transmit SNR. We call it “DNN-sd” where “sd” stands for *selective defense*.

Fig. 7 depicts the average MSE of our channel estimates. As shown in the figure, the DNN-based decoding, which is trained using error-free measurements, achieves almost the same performance as the search-based method at almost all SNR values. At very high SNR, however, the search method is better but the improvement is marginal (in the order of 10^{-3}). Interestingly, DNNs that are trained with noisy measurements (DNN-sd) outperforms both search and DNN. Nevertheless, we can see that at high SNR the DNN-sd’s MSE starts to saturate at $\approx 10^{-3}$ while the search method closes down the performance gap.

In Fig 6, we plot the *probability of error* associated with discovering at least k_i channel paths $\forall k_i = \{1, 2, 3\}$ (i.e., $1 - \mathbb{P}(k \geq k_i)$). In other words, we plot the probability of fewer than k_i discovered paths. This analysis shows that the probability of beam discovery for all three decoding methods are nearly the same except for two key observations: i) At low SNR, Fig. 6a shows a slightly better performance for DNN-sd against both search and DNN. ii) At high SNR, Figs. 6b and 6c show that the search method outperforms both DNN and DNN-sd although its MSE performance was inferior to that of DNN-sd. This could be explained by the fact that all the DNN models we use are trained to minimize the MSE and not directly trained for beam discovery. It also suggests that the *paths that were not correctly discovered must have very small gain values*, which makes them not very useful anyway.

2) *Finite Resolution ADC*: Now, we will shift our focus on finite resolution ADCs. Specifically, we will provide results for ADCs with $b=3, 5$, and 7-bit resolution and compare them against each other and against the ideal ADC case (with $b=\infty$). We only show the results for “DNN-sd” based decoding since the performance of the other two methods compare similarly to the trends of the ideal ADCs case shown above.

In Fig. 8a, we plot the MSE for various values of b . As expected, we can see that MSE is inversely proportional to resolution. We can also see that as SNR increases, higher

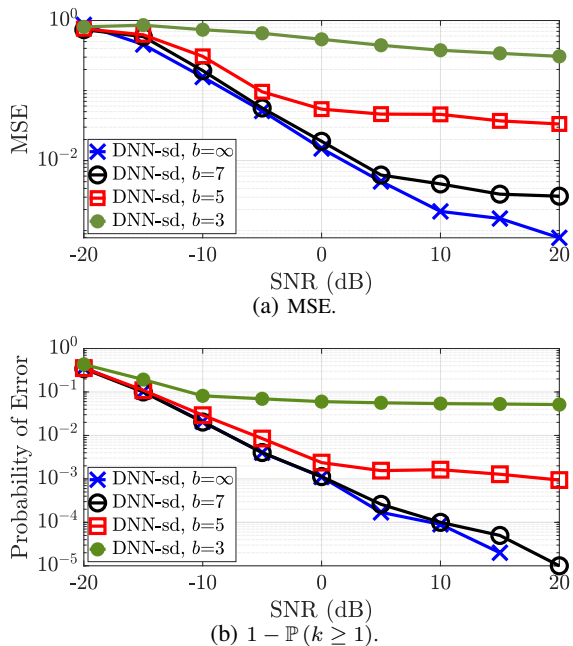


Fig. 8: Performance evaluation of various ADC resolutions

resolution is required to keep the MSE close to that of ideal ADCs. For instance, $b=5$ is reasonably good up to $\text{SNR} = -5\text{dB}$, while $b=7$ is very close to $b=\infty$ up to $\text{SNR} = 5\text{dB}$. Even at high SNR, the $b=7$ curve has a gap with ideal ADCs that is smaller than 5×10^{-3} . More crucially, the $b=7$ curve exhibits very close performance to ideal ADCs, in terms of path discovery, which is shown in Fig. 8b. Specifically, Fig. 8b shows the probability of misdetecting all paths and it follows similar performance trends as that of MSE.

E. Comparison With CS and IEEE 802.11ad

Our source-coding-based beam discovery is evaluated against CS based solutions and the IEEE 802.11ad beam alignment method. We use 15×31 single-path channels for this comparison. Recall that our solution requires 20 measurements for this channel (see Section VIII-B).

Compressed Sensing: We use a similar formulation for the mmWave channel estimation problem as in [21], [22]. The tx-precoders and rx-combiners are obtained using random, uniformly distributed phase shift values. That is, the components of all \mathbf{f}_j 's and \mathbf{w}_i 's are of the form $\exp(j\vartheta)$ where $\vartheta \sim [0, 2\pi)$. Fig. 9 shows the antenna pattern of \mathbf{w}_1 . For measurement decoding, we use the optimal l_0 -norm minimization problem [9]. This, in general, is too computationally complex to be of practical use. However, it provides an upper bound on the performance of other forms of sparse recovery algorithms like OMP, l_1 and l_2 -norm minimization, etc.

IEEE 802.11ad: We only consider the Sector Level Sweep stage of the channel estimation scheme of 802.11ad. At this stage, the TX starts by sequentially transmitting packets in all possible transmit AoDs (sectors) while the receiver performs quasi omni-directional reception. Then, the TX and RX switch roles where TX forms a quasi omni-directional antenna while RX sweeps through all possible receive AoAs (sectors). The

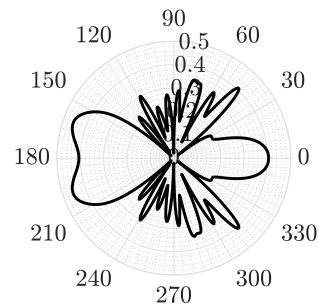


Fig. 9: Antenna pattern example at RX using Compressed Sensing.

directions that reveal the highest received signal strength is denoted as the AoA and AoD of the strongest channel path.

The beamwidth of the antenna patterns of our proposed scheme is quite different from that of the IEEE 802.11ad and that of CS. This results in different antenna gains in both schemes, and consequently different received SNR. Furthermore, a fixed transmit power for both schemes is not fair from a comparison standpoint due to their different number of measurements, which results in different levels of energy consumption. Thus, for comparison purposes, we opt to adjust the transmit power of each scheme such that *the total amount of energy consumption for the entire measurement process is fixed* for all schemes.

1) *Energy Calculation:* The energy consumption, denoted by E_T , is given by $E_T = m \times P_T \times \tau$, where m is the number of measurements, P_T is the total transmit power per measurement and τ is the time duration of one measurement. Since the antenna patterns at TX/RX of our proposed scheme consist of multiple overlapped beams (recall Fig. 2), the total power P_T is an integer multiple of the transmit power per direction/beam P , which depends on the number of overlapped beams at TX and RX. Let o_t and o_r denote the number of overlapped beams at the TX and RX, respectively. Hence, we have that $P_T = o_t \times o_r \times P$. We can further write the transmit power per beam as $P = \text{SNR} \frac{N_0}{\mu}$ (recall Eq. (11)). This gives us a total energy consumption (in millijoules (mJ)) for the entire measurement process as:

$$E_T = m \times o_t \times o_r \times \text{SNR} \frac{N_0}{\mu} \times \tau \quad (39)$$

Let $\mu = -88\text{dB}$ and $N_0 = 88\text{dBm}^7$. Finally, to find τ , we assume that a concatenation of Golay sequences of total length 1152 is used (similar to the channel estimation field of the IEEE 802.11ad), and is transmitted using *Differential Binary Phase Shift keying (DBPSK)* modulation, with symbol rate of 50 MSymbols/second. This gives us $\tau \approx 23\mu\text{s}$.

2) *Comparison Results:* Figs. 10a and 10b depict the simulation results for all three solutions. We plot the results against E_T , measured in millijoules. Recall that even though the total energy consumption is fixed, both our source coding

⁷ To find μ and N_0 , we assume a channel operating at a carrier frequency $f_c = 60$ GHz with bandwidth $B = 100$ MHz and distance between TX/RX of $d = 10\text{m}$. Further, we assume a receiver system with noise figure $\text{NF} = 6$ dB and temperature $T_0 = 293^\circ$ kelvin. The path loss constitutes both the free space path loss (FSPL) and atmospheric absorption. FSPL is given as: $\text{FSPL} = -10 \log_{10} \left(\frac{4\pi}{c} df_c \right)^{n_p}$, where $n_p = 2$ is the path loss exponent. Atmospheric absorption, however, can be ignored for small distances ($\leq 50\text{m}$) [35]. Hence, $\mu = \text{FSPL} = -88\text{dB}$. The noise power (in dBm) can be given as $N_0 = 10 \log_{10} (k_B T_0 B \times 1000) + \text{NF}$, where k_B is the Boltzmann constant.

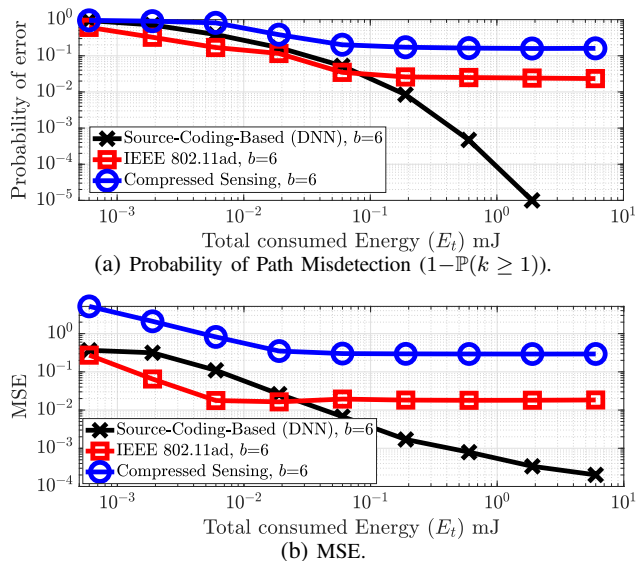


Fig. 10: Source Coding vs. Compressed Sensing vs. IEEE 802.11ad

and CS based methods *require* $\approx 57\%$ fewer measurements than is required by 802.11ad. For all schemes, we use ADCs with $b=6$ quantization bits. Fig. 10a shows the probability of path misdetection, which indicates that the CS solution performs the worst at all values of SNR. It also shows that at very low energy consumption, 802.11ad’s sector level sweep has slightly better performance than our proposed source-coding-based scheme. Nevertheless, the *probability of path misdetection is very high which makes path discovery unreliable in this region*. At higher values of energy, however, the quantization error causes the IEEE 802.11ad’s scheme to saturate at approximately 0.025, while our proposed scheme keeps improving. The better resilience our solution enjoys against quantization errors can be attributed to: i) the use of DNNs that are trained with quantized measurements, and ii) averaging the quantization error across multiple measurements in which the strong path is included. This is unlike 802.11ad’s approach which includes the strong channel path in just two measurements (once by sweeping through each of the TX/RX angular directions). Fig. 10b shows the average MSE, for which similar performance trends are observed.

IX. CONCLUSION

In this work, we treat the mmWave channel estimation problem a source compression problem. Our goal is to reconstruct the channel matrix using a small number of measurements. We exploit linear binary source codes for encoding the channel (do measurements) and a deep neural network based algorithm for measurement decoding (channel reconstruction). We are able, using a small number of measurements, to obtain high quality channel estimates. The lower bound on the achievable number of measurements is accurately characterized. Through simulation, the superiority of our proposed solution is demonstrated, in comparison to compressed-sensing-based solutions and IEEE 802.11ad’s beam alignment.

APPENDIX A PROOF OF LEMMA 2

Proof. Consider a set of n -dimensional linearly independent vectors, $\mathbf{v}_1, \dots, \mathbf{v}_m$ defined over \mathbb{F}_2 . Then, construct a matrix $\mathbf{M}_{\mathbb{F}_2}$ whose columns are $\mathbf{v}_1, \dots, \mathbf{v}_m$. Since \mathbf{v}_i ’s are independent, then $\mathbf{M}_{\mathbb{F}_2}$ has full column rank, i.e., $\mathbf{M}_{\mathbb{F}_2}$ is left-invertible over \mathbb{F}_2 ($m \leq n$). Thus $\mathbf{M}_{\mathbb{F}_2}$ has an $m \times m$ minor, call it $\mathbf{A}_{\mathbb{F}_2}$ whose determinant is non-zero. Now consider the matrix \mathbf{M} , defined over \mathbb{C} , whose elements are the 0 and 1 real scalars corresponding to $0_{\mathbb{F}_2}$ and $1_{\mathbb{F}_2}$ values of $\mathbf{M}_{\mathbb{F}_2}$. Let \mathbf{A} be its minor corresponding to $\mathbf{A}_{\mathbb{F}_2}$ of $\mathbf{M}_{\mathbb{F}_2}$. By lemma 5 (in Appendix B), we have $\det(\mathbf{A}) \neq 0$. Thus, \mathbf{M} is also left-invertible, hence its columns are linearly independent. \square

APPENDIX B LEMMA 5

Lemma 5. Let $\mathbf{A}_{\mathbb{F}}$ and \mathbf{A} be $n \times n$ matrices defined over \mathbb{F}_2 and \mathbb{R} , respectively. Let $a_{\mathbb{F}i,j}$, the elements of $\mathbf{A}_{\mathbb{F}}$, be scalars in $\{0_{\mathbb{F}_2}, 1_{\mathbb{F}_2}\}$, while $a_{i,j}$ the elements of \mathbf{A} , be scalars in $\{0, 1\} \subseteq \mathbb{R}$. Suppose that $\mathbf{A}_{\mathbb{F}}$ has non-zero determinant, i.e., $\det(\mathbf{A}_{\mathbb{F}}) \neq 0_{\mathbb{F}_2}$. If we define \mathbf{A} such that

$$a_{i,j} = \begin{cases} 0 & \text{if } a_{\mathbb{F}i,j} = 0_{\mathbb{F}_2} \\ 1 & \text{if } a_{\mathbb{F}i,j} = 1_{\mathbb{F}_2} \end{cases} \quad \forall 1 \leq i, j \leq n, \quad (40)$$

then, $\det(\mathbf{A}) \neq 0$.

Proof. Recall that the determinant of a square matrix defined over a commutative ring is given by the Leibniz formula [36]. Since \mathbb{F}_2 is a finite field (with 2 elements), it constitutes a commutative ring. Moreover, \mathbb{R} is a commutative ring [36]. Therefore, both determinants of $\mathbf{A}_{\mathbb{F}}$ and \mathbf{A} can be computed using the same exact formula. Since, finite field arithmetic over the prime field \mathbb{Z}_2 is the integers modulo 2, then we can write

$$\det(\mathbf{A}_{\mathbb{F}}) = \det(\mathbf{A}) \pmod{2} \quad (41)$$

Thus, $\exists q \in \mathbb{Z}$ (the set of integers), such that

$$\det(\mathbf{A}) = q \times 2 + \det(\mathbf{A}_{\mathbb{F}}) \quad (42)$$

$$= q \times 2 + 1 \quad (43)$$

were the last equation follows from the fact that $\det(\mathbf{A}_{\mathbb{F}}) \neq 0_{\mathbb{F}_2} \iff \det(\mathbf{A}_{\mathbb{F}}) = 1_{\mathbb{F}_2}$. Therefore, $\det(\mathbf{A})$ is an odd integer, which implies that $\det(\mathbf{A}) \neq 0$, concluding our proof. \square

APPENDIX C PROOF OF PROPOSITION 4

Proof. We will prove that adding an extra column $\mathbf{p} \in \mathbb{R}^m$ to any full rank matrix \mathbf{M} of size $m \times k$ with $m \leq k$ (i.e., $\text{rank}(\mathbf{M}) = m$) does not reduce its singular values.

Let $\mathbf{M}_{\mathbf{p}} = (\mathbf{M} \mid \mathbf{p})$ be an $m \times k+1$ matrix. Then, we can obtain the singular values of $\mathbf{M}_{\mathbf{p}}$ as the positive square roots of the eigenvalues of $\mathbf{M}_{\mathbf{p}}\mathbf{M}_{\mathbf{p}}^T$, which can be written as:

$$\mathbf{M}_{\mathbf{p}}\mathbf{M}_{\mathbf{p}}^T = (\mathbf{M} \mid \mathbf{p})(\mathbf{M} \mid \mathbf{p})^T \quad (44)$$

$$= \mathbf{M}\mathbf{M}^T + \mathbf{p}\mathbf{p}^T \quad (45)$$

Since $\mathbf{p}\mathbf{p}^T \succeq 0$ (i.e., positive semidefinite). Then, we have

$$\mathbf{M}_{\mathbf{p}}\mathbf{M}_{\mathbf{p}}^T - \mathbf{M}\mathbf{M}^T \succeq 0. \quad (46)$$

Let $\sigma_i(\cdot)$ denote the i^{th} largest singular value of a matrix. Then Eq. (46) implies

$$\begin{aligned} \sigma_i \left(\mathbf{M}_p \mathbf{M}_p^T \right) &\geq \sigma_i \left(\mathbf{M} \mathbf{M}^T \right) \quad \forall i = 1, \dots, m \quad (47) \\ \implies \sigma_{\min} \left(\mathbf{M}_p \mathbf{M}_p^T \right) &\geq \sigma_{\min} \left(\mathbf{M} \mathbf{M}^T \right) \implies \sigma_{\min} \left(\mathbf{M}_p \right) \geq \sigma_{\min} \left(\mathbf{M} \right) \quad (48) \end{aligned}$$

Define $\mathbf{G}^{(i)} \triangleq (\mathbf{g}_1 \mid \mathbf{g}_2 \mid \dots \mid \mathbf{g}_i)$, where \mathbf{g}_j is the j^{th} column of \mathbf{G} . Then, by sequentially applying the result shown in Eq. (48) (by adding columns of \mathbf{P} in Eq. (36)), we obtain

$$\begin{aligned} \sigma_{\min}(\mathbf{G}) &= \sigma_{\min}(\mathbf{G}^{(n)}) \geq \sigma_{\min}(\mathbf{G}^{(n-1)}) \geq \dots \\ &\geq \sigma_{\min}(\mathbf{G}^{(m+1)}) \geq \sigma_{\min}(\mathbf{G}^{(m)}) = \sigma_{\min}(\mathbf{I}_m) = 1 \quad \square \end{aligned}$$

REFERENCES

- [1] T. S. Rappaport, S. Sun, R. Mayzus, H. Zhao, Y. Azar, K. Wang, G. N. Wong, J. K. Schulz, M. Samimi, and F. Gutierrez, "Millimeter Wave Mobile Communications for 5G Cellular: It Will Work!" *IEEE Access*, vol. 1, pp. 335–349, 2013.
- [2] Z. Pi and F. Khan, "An Introduction to Millimeter-Wave Mobile Broadband Systems," *IEEE communications magazine*, vol. 49, no. 6, 2011.
- [3] M. R. Akdeniz, Y. Liu, M. K. Samimi, S. Sun, S. Rangan, T. S. Rappaport, and E. Erkip, "Millimeter Wave Channel Modeling and Cellular Capacity Evaluation," *IEEE journal on selected areas in communications*, vol. 32, no. 6, 2014.
- [4] "Cisco Visual Networking Index: Global Mobile Data Traffic Forecast Update, 2016 - 2021 White Paper," Mar 2017. [Online]. Available: <https://goo.gl/U1eQNM>
- [5] G. R. MacCartney, J. Zhang, S. Nie, and T. S. Rappaport, "Path Loss Models for 5G Millimeter Wave Propagation Channels in Urban Microcells," in *Globecom*, 2013, pp. 3948–3953.
- [6] S. Rangan, T. S. Rappaport, and E. Erkip, "Millimeter-Wave Cellular Wireless Networks: Potentials and Challenges," *Proceedings of the IEEE*, vol. 102, no. 3, pp. 366–385, 2014.
- [7] K. Haneda, J. Zhang, L. Tan, G. Liu, Y. Zheng, H. Asplund, J. Li, Y. Wang, D. Steer, C. Li *et al.*, "5G 3GPP-Like Channel Models for Outdoor Urban Microcellular and Macrocellular Environments," in *2016 IEEE 83rd Vehicular Technology Conference (VTC Spring)*. IEEE, 2016, pp. 1–7.
- [8] S.-E. Chiu, N. Ronquillo, and T. Javidi, "Active learning and csi acquisition for mmwave initial alignment," *IEEE Journal on Selected Areas in Communications*, vol. 37, no. 11, pp. 2474–2489, 2019.
- [9] J. W. Choi, B. Shim, Y. Ding, B. Rao, and D. I. Kim, "Compressed Sensing for Wireless Communications : Useful Tips and Tricks," *IEEE Communications Surveys Tutorials*, vol. PP, no. 99, pp. 1–1, 2017.
- [10] K. Venugopal, A. Alkhateeb, N. G. Prelcic, and R. W. Heath, "Channel estimation for hybrid architecture-based wideband millimeter wave systems," *IEEE Journal on Selected Areas in Communications*, vol. 35, no. 9, pp. 1996–2009, 2017.
- [11] A. Alkhateeb, O. El Ayach, G. Leus, and R. W. Heath, "Channel Estimation and Hybrid Precoding for Millimeter Wave Cellular Systems," *IEEE Journal of Selected Topics in Signal Processing*, vol. 8, no. 5, pp. 831–846, 2014.
- [12] J. Rodríguez-Fernández, N. González-Prelcic, K. Venugopal, and R. W. Heath, "Frequency-Domain Compressive Channel Estimation for Frequency-Selective Hybrid Millimeter Wave MIMO Systems," *IEEE Transactions on Wireless Communications*, vol. 17, no. 5, pp. 2946–2960, 2018.
- [13] H. Hassanieh, O. Abari, M. Rodriguez, M. Abdelghany, D. Katabi, and P. Indyk, "Fast Millimeter Wave Beam Alignment," in *Proceedings of the 2018 Conference of the ACM Special Interest Group on Data Communication*. ACM, 2018.
- [14] X. Li and A. Alkhateeb, "Deep Learning for Direct Hybrid Precoding in Millimeter Wave Massive MIMO Systems," *arXiv preprint arXiv:1905.13212*, 2019.
- [15] H. He, C.-K. Wen, S. Jin, and G. Y. Li, "Deep Learning-Based Channel Estimation for Beamspace mmWave Massive MIMO Systems," *IEEE Wireless Communications Letters*, vol. 7, no. 5, pp. 852–855, 2018.
- [16] H. Huang, J. Yang, H. Huang, Y. Song, and G. Gui, "Deep Learning for Super-Resolution Channel Estimation and DOA Estimation Based Massive MIMO System," *IEEE Transactions on Vehicular Technology*, vol. 67, no. 9, 2018.
- [17] A. Alkhateeb, S. Alex, P. Varkey, Y. Li, Q. Qu, and D. Tujkovic, "Deep Learning Coordinated Beamforming for Highly-Mobile Millimeter Wave Systems," *IEEE Access*, vol. 6, pp. 37 328–37 348, 2018.
- [18] Y. Shabara, C. E. Koksals, and E. Keci, "Beam discovery using linear block codes for millimeter wave communication networks," *IEEE/ACM Transactions on Networking*, vol. 27, no. 4, pp. 1446–1459, Aug 2019.
- [19] J. Li, Y. Sun, L. Xiao, S. Zhou, and C. E. Koksals, "Analog Beam Tracking in Linear Antenna Arrays: Convergence, Optimality, and Performance," in *2017 51st Asilomar Conference on Signals, Systems, and Computers*. IEEE, 2017.
- [20] M. Hashemi, A. Sabharwal, C. E. Koksals, and N. B. Shroff, "Efficient Beam Alignment in Millimeter Wave Systems Using Contextual Bandits," in *IEEE INFOCOM 2018-IEEE Conference on Computer Communications*. IEEE, 2018.
- [21] A. Alkhateeb, G. Leusz, and R. W. Heath, "Compressed Sensing Based Multi-User Millimeter Wave Systems: How Many Measurements Are Needed?" in *2015 IEEE International Conference on Acoustics, Speech and Signal Processing (ICASSP)*, April 2015, pp. 2909–2913.
- [22] X. Lu, W. Yang, Y. Cai, and X. Guan, "Comparison of CS-Based Channel Estimation for Millimeter Wave Massive MIMO Systems," *Applied Sciences*, vol. 9, no. 20, p. 4346, 2019.
- [23] C.-K. Wen, C.-J. Wang, S. Jin, K.-K. Wong, and P. Ting, "Bayes-Optimal Joint Channel-and-Data Estimation for Massive MIMO with Low-Precision ADCs," *IEEE Transactions on Signal Processing*, vol. 64, no. 10, pp. 2541–2556, 2016.
- [24] J. Mo, P. Schniter, and R. W. Heath, "Channel Estimation in Broadband Millimeter Wave MIMO Systems with Few-Bit ADCs," *IEEE Transactions on Signal Processing*, vol. 66, no. 5, pp. 1141–1154, 2018.
- [25] W. Ma, C. Qi, Z. Zhang, and J. Cheng, "Deep Learning for Compressed Sensing Based Channel Estimation in Millimeter Wave Massive MIMO," in *2019 11th International Conference on Wireless Communications and Signal Processing (WCSP)*. IEEE, 2019, pp. 1–6.
- [26] T. Wang, C.-K. Wen, H. Wang, F. Gao, T. Jiang, and S. Jin, "Deep Learning for Wireless Physical Layer: Opportunities and Challenges," *China Communications*, vol. 14, no. 11, pp. 92–111, 2017.
- [27] D. Tse and P. Viswanath, *Fundamentals of Wireless Communication*. Cambridge university press, 2005.
- [28] J. Mo, P. Schniter, N. G. Prelcic, and R. W. Heath, "Channel Estimation in Millimeter Wave MIMO systems with one-bit quantization," in *2014 48th Asilomar Conference on Signals, Systems and Computers*, Nov 2014, pp. 957–961.
- [29] M. Kokshoorn, H. Chen, P. Wang, Y. Li, and B. Vucetic, "Millimeter Wave MIMO Channel Estimation Using Overlapped Beam Patterns and Rate Adaptation," *IEEE Transactions on Signal Processing*, vol. 65, no. 3, pp. 601–616, Feb 2017.
- [30] D. P. Kingma and J. Ba, "Adam: A Method for Stochastic Optimization," *arXiv preprint arXiv:1412.6980*, 2014.
- [31] F. Chollet *et al.*, "Keras," <https://keras.io>, 2015.
- [32] Y. Shabara. (2019) Simulation Codes for Source-Coding-Based Beam Discovery. [Online]. Available: https://github.com/yahiaShabara/sourceCoding_beamD
- [33] M. Abadi, P. Barham, J. Chen, Z. Chen, Davis *et al.*, "Tensorflow: A System for Large-Scale Machine Learning," in *12th {USENIX} Symposium on Operating Systems Design and Implementation ({OSDI} 16)*, 2016.
- [34] S. Sur, X. Zhang, P. Ramanathan, and R. Chandra, "BeamSpy: Enabling Robust 60 GHz Links Under Blockage," in *13th {USENIX} Symposium on Networked Systems Design and Implementation ({NSDI} 16)*, 2016.
- [35] A. Tomkins, A. Poon, E. Juntunen, A. El-Gabaly, G. Temkine, Y.-L. To, C. Farnsworth, A. Tabibiazar, M. Fakhrazadeh, S. Jafarlou *et al.*, "A 60 GHz, 802.11 ad/WiGig-Compliant Transceiver for Infrastructure and Mobile Applications in 130 nm SiGe BiCMOS," *IEEE Journal of Solid-State Circuits*, vol. 50, no. 10, pp. 2239–2255, 2015.
- [36] D. Grinberg, "Notes On the Combinatorial Fundamentals of Algebra," 2016.